Journal of Structural Geology, Vol. 12, No. 7, pp. 903 to 910, 1990
Printed in Great Britain

0191-8141/90 $03.00+0.00

Fault-propagation folds above thrusts with constant dip

J. S. CHESTER

Center for Tectonophysics and Department of Geology, Texas A & M University, College Station, TX 77843, U.S.A.

and

F. M. CHESTER*

Lamont-Doherty Geological Observatory, Palisades, NY 10964, U.S.A.

(*Received* 7 *February* 1989; *accepted in revised form* 30 *January* 1990)

Abstract—Previous models of fault-propagation folds have been extended to include the case where folding initiates above a thrust ramp of constant dip. The model may be useful in analyses of fold-thrust structures in thin- and thick-skinned compressional terrains. It may be most applicable to fault-propagation folds that develop as a fault propagates from a thick, massive, brittle unit into a thinly layered, anisotropic unit.

INTRODUCTION

IN compressional terrains that are characterized by parallel folding and bedding-plane slip, fold-thrust structures may be described geometrically as fault-bend folds, fault-propagation folds and detachment folds (Suppe 1983, Suppe & Medwedeff 1984, Jamison 1987). In many cases, geometric models based on line-length and area balancing can facilitate interpretation of these structures in the subsurface.

The purpose of this paper is to extend the geometric analyses available for fault-propagation folds (Suppe 1985, Jamison 1987). A fault-propagation fold develops concurrently with and immediately above a propagating fault. It is directly associated with an underlying ramp segment of a thrust fault, being the macroscopic response of the overlying units to displacement on the thrust (e.g. Williams & Chapman 1983). Previous models have considered the case where folding initiates as a thrust propagates out of a décollement (Fig. 1a). These models are based on the assumptions of plane strain, constant area and bed-length, and parallel, kink-style folding. The models provide specific relationships between fold and fault geometry. Jamison (1987) showed how the assumption of constant bed thickness and parallel folding can be relaxed to allow thinning or thickening of the frontal fold limb.

In all previous models, fault-propagation folding initiates at a bend in the fault surface, and accordingly, all layers in the hanging wall cut by the fault are folded through the anticlinal axial surface A (Fig. 1a). Motivated by observations of natural and model fault-propagation folds (Chester *et al.* 1986, Chester 1988), we extend the earlier geometric analyses to include the case in which folding initiates above a thrust ramp of constant dip (Fig. 1b). The important aspects of this generalized

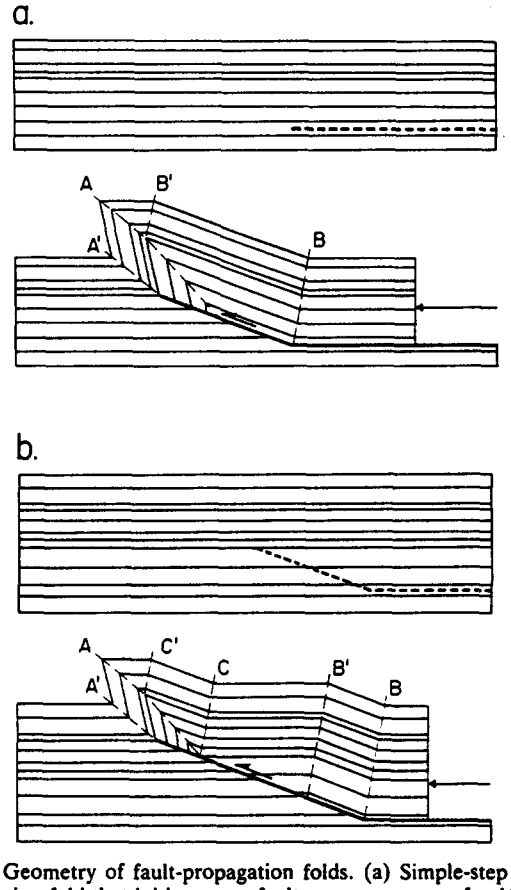

Fig. 1. Geometry of fault-propagation folds. (a) Simple-step fault-propagation fold that initiates as a fault propagates out of a décollement (modified after Suppe & Medwedeff 1984). (b) Fault-propagation fold that initiates above a fault or fracture of constant dip. Note that the fault-propagation fold in (b) between the axial surfaces A′ and C is separate from the fault-bend fold (B–B′) at the lower ramp hinge, whereas in (a) the fault-bend and fault propagation folds are combined in a single structure.

*Present address: Department of Earth and Atmospheric Sciences, St. Louis University, St. Louis, MO 63103, U.S.A.

model are that it can describe a fault-propagation fold that is not associated with a fault bend, and in which some of the lower layers in the hanging wall cut by the fault are not folded through the anticlinal axial surface A (Fig. 1b). This type of fault-propagation folding is compatible with models describing the propagation of existing, isolated thrust fault ramp segments (e.g. Eisenstadt & De Paor 1987) and the propagation of thrust faults upsection from décollements at depth (e.g. Rich 1934). Application of the model is illustrated with an analysis of an exposed mesoscopic fold-thrust structure from the Appalachian fold and thrust belt. An example of how this model may be used for subsurface analysis is illustrated with a fold above a basement thrust in the Wyoming Foreland.

MODEL GEOMETRY

The fault-propagation fold consists of two intersecting kink-bands A–A′ and C–C′ (Fig. 2). Axial surface C is fixed with respect to the hanging wall and intersects the fault at the fold initiation point (P) in the hanging wall. Thrust displacement decreases from f_0 at the fold initiation point to zero at the fault tip. The axial surfaces B and B′ constitute a fault-bend fold associated with the ramp–flat intersection. The fault-bend fold is separated from the fault-propagation fold by the unfolded region between axial surfaces C and B′. The fault-bend fold may be analyzed independently (Suppe 1983) and is not considered further. The distance from the fault tip to the fold initiation point, and the width of the kink-bands A–A′, B–B′ and C–C′, increase as the magnitude of slip increases (Fig. 3).

The geometry shown in Fig. 2 is based on the assumptions of: (1) plane strain; (2) conservation of cross-sectional area; (3) conservation of line-length except in the forelimb of the fold; and (4) parallel kink-folding. We relax the assumptions of constant line length to allow thickening or thinning in the frontal fold limb because this is observed in many natural cases (Jamison 1987). As shown in Fig. 2, and derived in the Appendix, the angles (γ_1) and (γ_2) are related to the interlimb angle (γ) by

$$\gamma = \gamma_1 + \gamma_2, \tag{1}$$

and to the thickening of the forelimb (tf/t) by

$$tf/t = \sin\gamma_2/\sin\gamma_1 \tag{2}$$

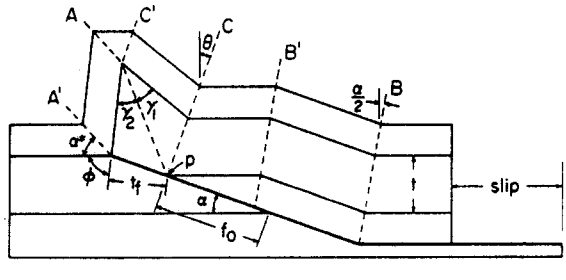

Fig. 2. Diagram of a fault-propagation fold defining the variables of the geometric model.

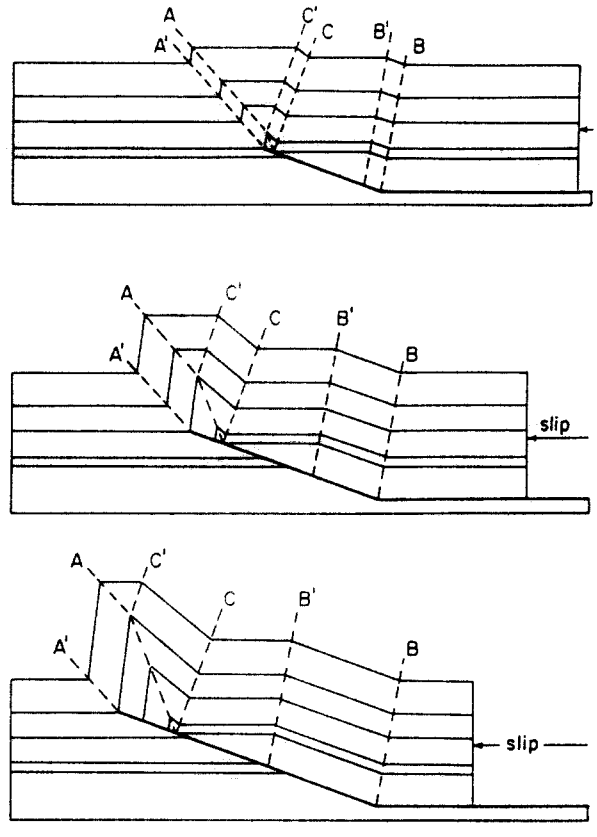

Fig. 3. Geometry of a fault-propagation fold with $\alpha = 20°$, $\theta = 10°$, $tf/t = 1$ and $\gamma = 56°$ for three magnitudes of fault slip.

(e.g. Jamison 1987, equation 7). Conservation of area in the layer that is both cut by the fault and folded through axial surface A is given by

$$\cot\gamma_1 - \cot\alpha - 2\tan\theta + (tf/t)^2[\cot\gamma_2 - \cot(2\theta + \gamma - \alpha)] = 0. \tag{3}$$

Geometries that satisfy equations (1), (2) and (3) are viable. By combining these equations the geometry of the fault-propagation fold may be completely specified by the ramp dip (α), interlimb angle (γ), back limb dip (2θ) and thickening of the frontal fold limb (tf/t) according to:

$$\cot\alpha + 2\tan\theta - \cot\gamma - 2(tf/t)\csc\gamma + (tf/t)^2[\cot(2\theta + \gamma - \alpha) - \cot\gamma] = 0. \tag{4}$$

Assuming that the frontal fold limb thickens uniformly, the dip (α^*) of axial surfaces A and A′ in the unfaulted layers is given by

$$\cot\alpha^* = (tf/t)\csc(2\theta + \gamma) + \cot(2\theta + \gamma). \tag{5}$$

The dip of the frontal fold limb is equivalent to the supplement to the sum of the interlimb angle and back limb dip (see Appendix, equation A6).

In this model, the back limb dip (2θ) is not necessarily equal to the ramp dip (α). Thus, for specified ramp and back limb dips there exists a family of solutions for interlimb angle as a function of the thickening of the frontal fold limb (Fig. 4). Similarly, for a specified ramp dip and forelimb thickening there is a family of solutions for interlimb angle as a function of the back limb dip (Fig. 5). For some values of α, γ and tf/t, there are two

values of θ that satisfy equation (4), which is illustrated graphically by the crossing of curves in Fig. 5.

For all solutions, the thickness (t) of the layer that is both faulted and folded through axial surface A is proportional to the fault offset (f_o) measured at the fold-initiation point (Fig. 2) according to:

$$f_o/t = \csc\ \alpha - (tf/t)\csc(2\theta + \gamma - \alpha). \quad (6)$$

The left-hand side of equation (6) approaches zero with an increase in interlimb angle and ramp dip. Accordingly, high-angle reverse faults propagate a great distance relative to fault offset and show less associated folding than low-angle thrusts.

Although the model provides viable solutions for many ramp dips and interlimb angles, not all solutions are geologically reasonable. For example, low-angle thrusts with large back limb dips require folds verging opposite to the thrust. Generally, admissible solutions are those for ramps and back limbs dipping less than approximately 45° and interlimb angles that are less than approximately 120°.

COMPARISON WITH PREVIOUS MODELS

The previous simple-step fault-propagation fold models are based on the assumption that folding initiates as a propagating fault steps up out of a décollement into a ramp orientation; the fold nucleating at the step (Suppe & Medwedeff 1984, Suppe 1985, Jamison 1987). These models are special cases of the present model. The generalized model presented here assumes folding also can nucleate as an existing fault ramp (or fracture) is extended in the same plane (Fig. 1b). Thus the model allows for the presence of faulted beds in the hanging wall below the fold initiation point and a back limb dip that is different from the ramp dip. The model does not require that the ramp root into a flat, and therefore may be compatible with the model for ramp development proposed by Eisenstadt & De Paor (1987). In their model thrust ramps form first in the most competent layers, and then are linked by upward and downward propagation to form the ramp–flat geometry. Extension of these early-formed ramps into structural lithic units with better layering or less competence could lead to the fault-propagation fold geometry described by the model presented here. Such a kinematic development and resultant geometry have been produced in rock model experiments of fold-thrust structures (Chester *et al.* 1986). In the experiments, fault-propagation folding initiates as a pre-existing ramp propagates up section across a mechanical layer boundary from a relatively thick, strong, brittle unit into a thinly-layered, mechanically anisotropic or ductile unit.

If the fold initiation point (P) in the hanging wall originates at the base of the ramp and the back limb dip is equal to the ramp dip ($2\theta = \alpha$), the axial surfaces B′ and C (Fig. 2) are not required and the general model reduces to the simple-step fault-propagation fold described by Suppe & Medwedeff (1984) (Fig. 1a). For the case with no thickening or thinning of the forelimb ($tf/t = 1$), equation (2) requires $\gamma_1 = \gamma_2$, and the geometric relation (4) defining the fault-propagation fold reduces to

$$(1 + 2\cos^2\gamma_1)/\sin(2\gamma_1) = (2 - \cos\alpha)/\sin\alpha \quad (7)$$

(see Appendix). In this case there is a unique relationship between ramp dip and interlimb angle (fig. 9-50 of Suppe 1985). If thickness changes are allowed in the forelimb of a simple-step fault-propagation fold, equation (4) becomes

$$\cot\gamma - 2\cot\gamma_1 + (2 - \cos\alpha)/\sin\alpha = 0 \quad (8)$$

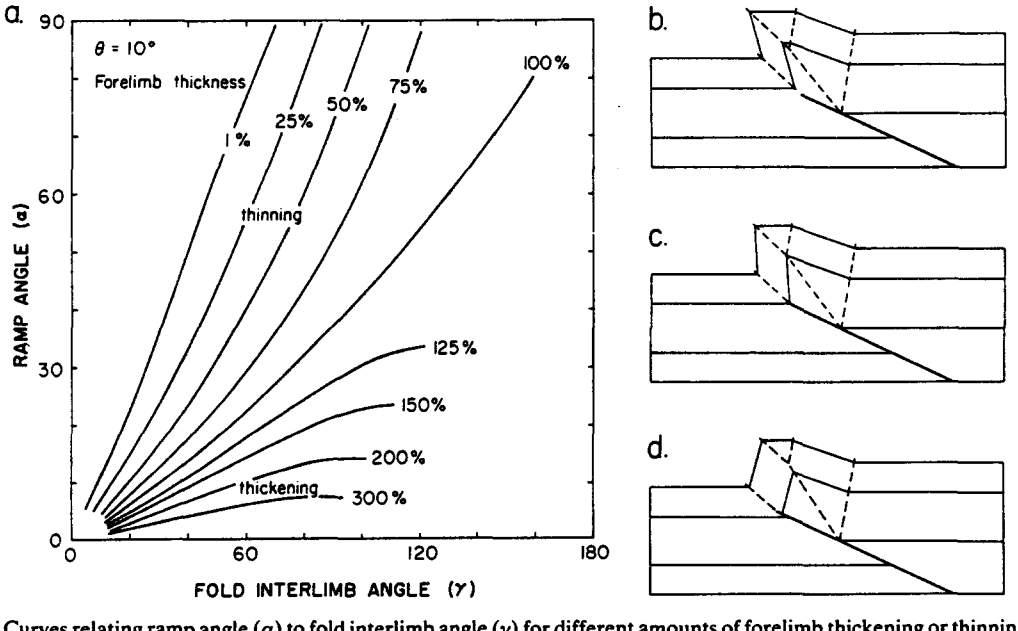

Fig. 4. (a) Curves relating ramp angle (α) to fold interlimb angle (γ) for different amounts of forelimb thickening or thinning (tf/t) and for $\theta = 10°$. Geometry of fault-propagation folds for $\alpha = 25°$, $\theta = 10°$ and forelimb thickening of (b) $tf/t = 0.75$, (c) $tf/t = 1.0$ and (d) $tf/t = 1.25$.

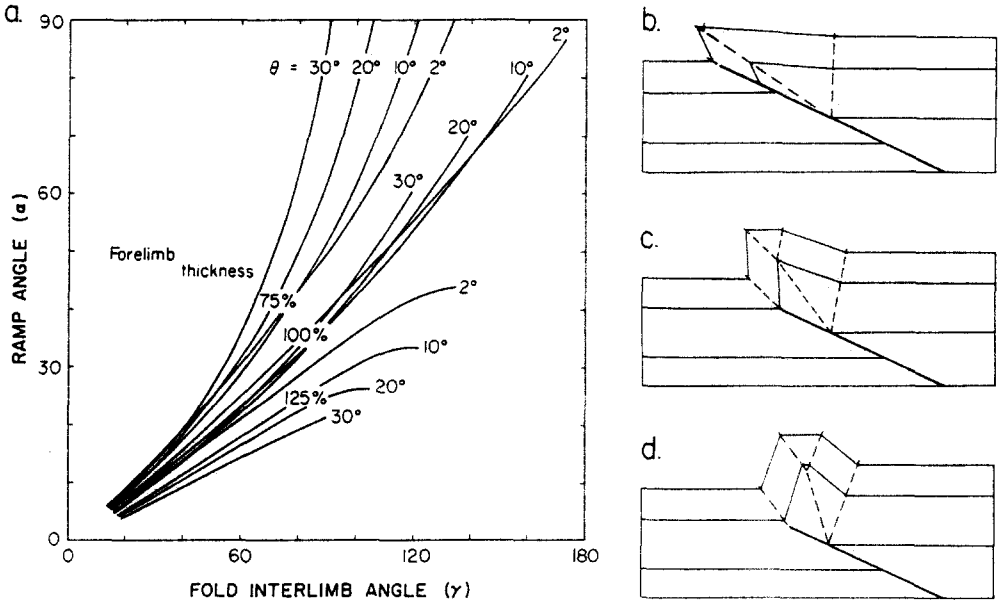

Fig. 5. (a) Curves relating ramp angle (α) to fold interlimb angle (γ) for different θ and for different forelimb thickening (tf/t) of 0.75, 1.0 and 1.25. Curves for $\theta = 2°$ show solutions for very shallow but non-zero back limb dips. Geometry of fault-propagation folds for $\alpha = 25°$, $tf/t = 1.0$, and (b) $\theta = 2°$, (c) $\theta = 10°$ and (d) $\theta = 20°$.

as derived by Jamison (1987, equation 11) (see Appendix).

NATURAL EXAMPLES

Two examples of fault-cored folds are presented to illustrate the application of this model. The first example is a mesoscopic fault-propagation fold in which both the fold and fault are exposed. This offers a type example of the geometry described in this paper, i.e. a fault-propagation fold that developed above a thrust of constant dip. The second example is a macroscopic fold over a thrust in crystalline basement. This latter example is used to illustrate the application of the model to subsurface analysis where data are limited.

Mesoscopic example

The fault-propagation fold is located in the Cumberland Plateau décollement zone, and is exposed in a large road cut along Route 8 near Dunlap, Tennessee. The entire road cut has been mapped by Harris & Milici (1977), and the fold and surrounding structure is presented in a down-plunge projection by Wojtal (1986). The fold occurs in interbedded sandstones, siltstones and shales of the Gizzard Group. Several photographs of the fold have been published (Serra 1977, Suppe 1985, Boyer 1986), and Serra (1977, 1978) presents a detailed tracing of the fault–fold structure from a composite of serial photographs.

The road cut crosses the structure oblique to the transport direction. We have constructed a down-plunge projection of the fold based on the tracing of Serra (1978) and our field measurements that define the dimension and orientation of the outcrop and structural elements (Fig. 6a). There is some distortion inherent in a tracing from serial photographs, but the accuracy is sufficient for the purposes of this analysis.

The fault makes an angle with bedding of approximately 17.5° in the footwall and hanging wall below the fold initiation point (Fig. 6a). In our projection the fault tip is located where truncation and offset of bedding along the fault is negligible. The fault may continue beyond this point parallel to bedding and define an upper flat. However, there is no evidence for large transport of the hanging wall along a flat, nor any indication of the relative timing of the formation of the fold and upper flat. An estimate of the magnitude of slip on the main fault below the fold may be obtained from the offset of a bedding horizon identified by small sandstone lenses (Fig. 6a). The down-plunge projection of Wojtal (1986) indicates that the thrust ramp extends at nearly the same orientation to lower structural levels before merging with a bedding-parallel décollement.

The fact that the fold occurs above a thrust, that the displacement on the thrust decreases upwards in the folded region, and that the footwall is not folded, suggests this fold may be described as a fault-propagation fold. However, the structure cannot be described by previous geometric models of a simple-step fault-propagation fold out of a décollement because the fault has a relatively uniform dip in the vicinity of the fold initiation point, the bedding cut-off angles of the hanging wall and footwall below the folded layers are the same, and the lower layers of the hanging wall are not folded (Fig. 1). These are the essential features of the geometric model presented here (Fig. 2).

We fit the geometry of the fault–fold structure with the geometric model by using a ramp dip (α) of 17.5° (relative to bedding) and varying the other parameters. The best-fit is obtained for a back limb dip (2θ) of 25°, interlimb angle (γ) of 97°, and thickening of the forelimb (tf/t) of 1.67 (Fig. 6b). It is clear that the geometric

model does not fit the natural structure exactly. This is because several aspects of the natural structure are not treated in the geometric model. In particular, the rock unit is not thinly- or uniformly-layered with respect to the size of the structure, it does not deform solely by distributed layer-parallel shear or form perfect kink-fold hinge geometries at this scale, there is a minor thickening by faulting and folding in the hanging wall, and the thickening in the forelimb of the fold is considerably greater in the shale than in the sandstone beds. In addition, the structure varies along strike which suggests that the model solution will also vary along strike. Nevertheless, the overall geometry of the fold–thrust structure, including the magnitude of offset along the fault at the fold initiation point (f_o), is described satisfactorily by this geometric model and not by the previous models (Fig. 6b). This result suggests that the geometric model may be useful for the analysis of similar fault-propagation fold structures in the subsurface where data are more limited.

Macroscopic example

The Pitchfork Anticline is a Laramide fold in Paleozoic rocks of the Bighorn Basin, Wyoming. The geometry of this fold in the subsurface is constrained by surface mapping, well and seismic data (Fig. 7a). For this analysis, thicknesses of the stratigraphic units, bedding dips and the location of contacts, small faults and fold axes are taken from the surface and well data provided by Peterson (1983). A seismic reflection profile across the structure suggests that the Precambrian basement surface has a uniform regional dip of 7° to the east, except directly below the fold where it is offset along a relatively discrete fault zone (R. R. Gries personal communication, 1989). The seismic and surface data suggest that the uplift of the basement surface along this fault is of the order of 550 m.

These structural data suggest that the Pitchfork Anticline formed by shortening of the sedimentary rocks above a basement thrust, but are insufficient to define the fold geometry in detail or the attitude of the fault (Fig. 7a). The rock units involved in the deformation may be described mechanically as an isotropic, brittle unit (basement) overlain by a relatively thinly layered, anisotropic unit (sedimentary cover). We consider the possibility that the Pitchfork Anticline is a fault-propagation fold in which the folding nucleated at the mechanical boundary between the basement and sedimentary cover, and that the subsurface geometry can be constrained by the geometric model.

The best-fit to the available structural data is given by

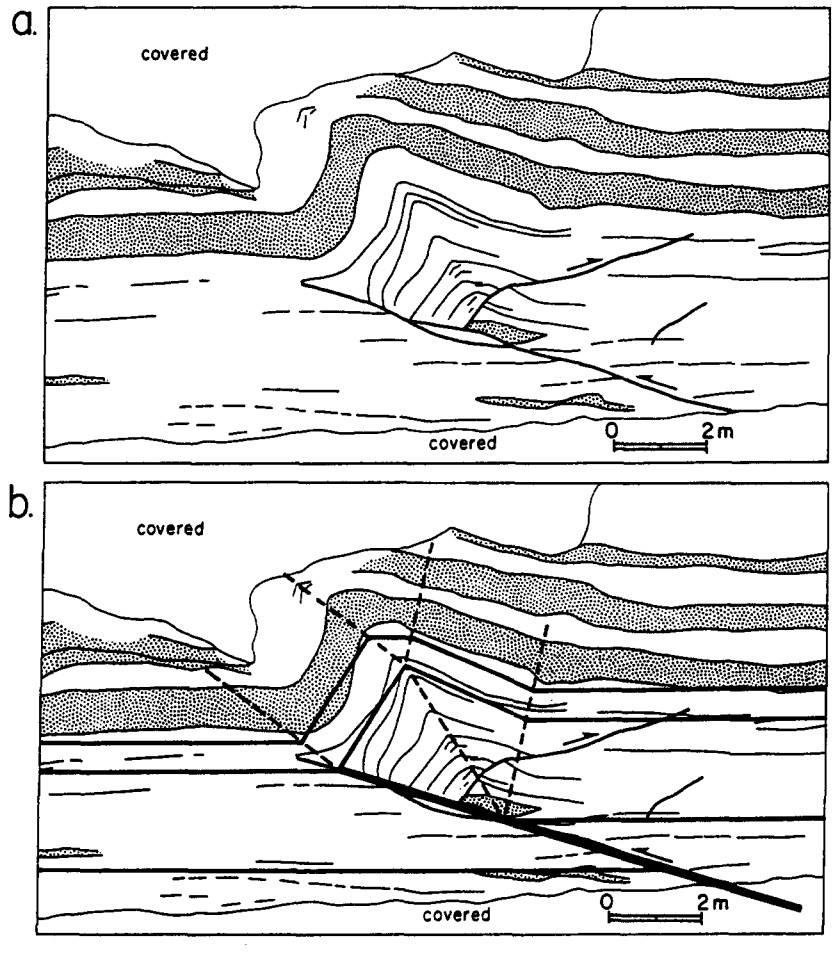

Fig. 6. (a) Down-plunge projection of the fault-propagation fold in the Cumberland Plateau décollement zone, Tennessee, based on field measurements and a tracing of serial photographs by Serra (1978). Thin lines are bedding planes, thick lines are faults and stippling represents sandstone beds. The boundaries of the exposure are indicated. (b) The best-fit of the model to the fault–fold structure is given by $\alpha = 17.5°$, $2\theta = 25°$, $\gamma = 97°$ and thickening (tf/t) of 1.67.

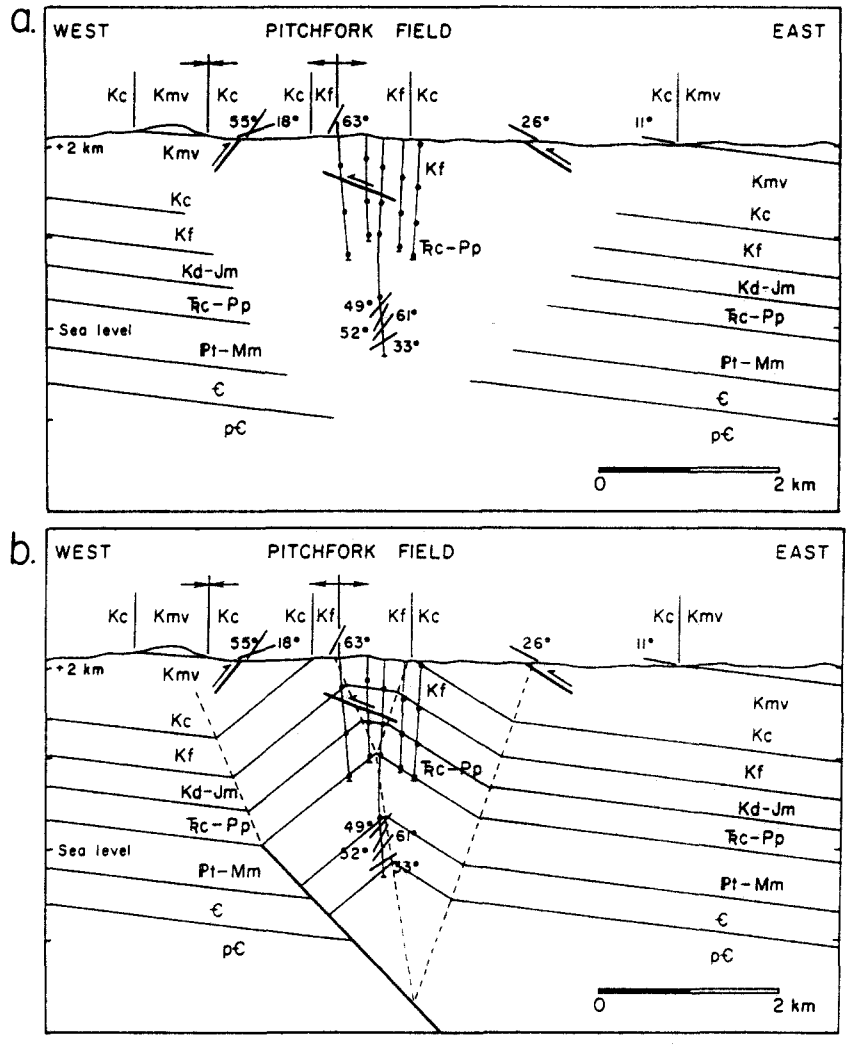

Fig. 7. (a) Structural data for the Pitchfork Anticline, Bighorn Basin, Wyoming. Surface and well data are taken from Peterson (1983). Seismic reflection data are used to constrain the regional dip and magnitude of fault offset (R. R. Gries personal communication, 1989). (b) Structural interpretation of the fold based on the geometric model. The sedimentary bedding horizons are represented approximately with straight lines and a kink-fold geometry. The best-fit is given by $\gamma = 110°$, $2\theta = 24°$, $\alpha = 38°$ and thickening (tf/t) of 1.13.

forelimb thickening (tf/t) of 1.13, an interlimb angle of 110°, back limb dip of 31° ($\theta = 12°$) and a fault dip of 45° ($\alpha = 38°$, Fig. 7b). As with the previous example, the model describes the overall geometry of the structure and satisfies the structural data adequately, but it does not predict minor deformational features within the structure such as the smaller fault known to exist in the core of the fold (Fig. 7a).

The model does not indicate that the fold initiation point is located at the contact between the basement and sedimentary rock, but instead suggests that some of the basement in the Pitchfork structure has undergone kink-style folding. Although this style of deformation is present in some Laramide structures, it is not ubiquitous (e.g. Stearns 1971, Chase *et al.* 1989). Therefore it may be appropriate to supplement this analysis of the Pitchfork Anticline using other models for basement fault geometries such as that described by Narr & Suppe (1989) or to add minor deformational features characteristic of basement-cored folds of the Wyoming foreland (e.g. Stearns 1971, Brown 1989). Nevertheless, this example demonstrates that the geometric model can provide a first step in the analysis of a subsurface fault-propagation fold structure by defining a fault orientation and an overall fold geometry that is balanced.

SUMMARY AND CONCLUSIONS

We have extended geometric models of fault-propagation folds to include the case of folding during propagation of a thrust ramp without a change in fault orientation. The model defines relationships between interlimb angle and fault dip for various forelimb thickness variations and back limb dips. The simple-step (out of a décollement) fault-propagation fold is a specific case of the present model.

We show natural examples of folds that may be described by the present model. Even so, the geometric model cannot be applied indiscriminately. The application requires evaluation of the assumptions of the geometric analysis in light of each natural case.

The present model may be particularly well-suited for

the analysis of fault-propagation folds that initiate as a fault encounters a change in mechanical stratigraphy, such as a contact between a massive, isotropic, brittle unit, and a thinly layered, anisotropic unit. In this sense, it may best describe folds within thin-skinned thrust belts having contrasting structural lithic units, or mesoscopic and macroscopic folds in sedimentary rock above basement thrusts.

Acknowledgements—We thank W. R. Jamison, J. H. Spang and the Journal reviewers for helpful comments concerning the manuscript, and W. G. Brown and R. R. Gries for discussing the interpretation of seismic and other data for the Pitchfork anticline. This work was supported by grants to J. S. Chester by ARCO Oil and Gas Company, Amoco Production Company and Chevron U.S.A. Inc., and a Lamont-Doherty Postdoctoral Fellowship awarded to F. M. Chester.

REFERENCES

Boyer, S. E. 1986. Styles of folding within thrust sheets: examples from the Appalachian and Rocky Mountains of the U.S.A. and Canada. *J. Struct. Geol.* **8**, 325–339.

Brown, W. G. 1989. Deformational style of Laramide uplifts in the Wyoming foreland. In: *Interaction of the Rocky Mountain Foreland and the Cordilleran Thrust Belt* (edited by Schmidt, C. J. & Perry, W. J., Jr). *Mem. geol. Soc. Am.* **171**, 1–25.

Chase, R. B., Schmidt, C. J., Nelson, G. C., Genovese, P. W. & Edgar, C. J. 1989. Mechanical behaviors of basement rocks in Rocky Mountain Foreland folds. *Geol. Soc. Am. Abs. w. Prog.* **21**, A137.

Chester, J. S. 1988. Geometry and fracture distribution in fault-propagation folds in nature and experiments. *Abs. Am. Ass. Petrol. Geol.* **72**, 171.

Chester, J. S., Logan, J. M. & Spang, J. H. 1986. Role of layering in the deformation of thrust sheets. *Geol. Soc. Am. Abs. w. Prog.* **18**, 346.

Eisenstadt, G. & De Paor, D. G. 1987. Alternative model of thrust-fault propagation. *Geology* **15**, 630–633.

Harris, L. D. & Milici, R. C. 1977. Characteristics of thin-skinned style of deformation in the southern Appalachians, and potential hydrocarbon traps. *Prof. Pap. U.S. geol. Surv.* **1018**.

Jamison, W. J. 1987. Geometric analysis of fold development in overthrust terrains. *J. Struct. Geol.* **9**, 207–219.

Narr, W. & Suppe, J. 1989. Kinematics of low temperature, basement involved compressive structures. *Geol. Soc. Am. Abs. w. Prog.* **21**, A137.

Peterson, F. A. 1983. Foreland detachment structures. In: *Rocky Mountain Foreland Basins and Uplifts* (edited by Lowell, J. D. & Gries, R. R.). *Rocky Mountain Ass. Geol.*, 65–77.

Rich, J. L. 1934. Mechanics of low-angle overthrust faulting as illustrated by Cumberland thrust block, Virginia, Kentucky, and Tennessee. *Bull. Am. Ass. Petrol. Geol.* **18**, 1584–1587.

Serra, S. 1977. Styles of deformation in the ramp regions of overthrust faults. *Wyoming Geol. Ass. 29th Annual Field Conf. Guidebook*, 487–498.

Serra, S. 1978. Styles of deformation in the ramp regions of overthrust faults. Unpublished Ph.D. thesis, Texas A & M University, College Station, Texas.

Stearns, D. W. 1971. Mechanisms of drape folding in the Wyoming Province. *Wyoming Geol. Ass. 23rd Annual Field Conf. Guidebook*, 125–143.

Suppe, J. 1983. Geometry and kinematics of fault-bend folding. *Am. J. Sci.* **283**, 684–721.

Suppe, J. 1985. *Principles of Structural Geology*. Prentice-Hall, Englewood Cliffs, New Jersey.

Suppe, J. & Medwedeff, D. A. 1984. Fault-propagation folding. *Geol. Soc. Am. Abs. w. Prog.* **16**, 670.

Williams, G. & Chapman, T. 1983. Strains developed in the hanging walls of thrusts due to their slip-propagation rate: a dislocation model. *J. Struct. Geol.* **5**, 563–571.

Wojtal, S. 1986. Deformation within foreland thrust sheets by populations of minor faults. *J. Struct. Geol.* **8**, 341–360.

APPENDIX

Derivation of model equations

Equation (2) is derived by expressing the length of line SP in terms of γ_1 and γ_2 (Fig. A1):

$$SP = tf/\sin\gamma_2 = t/\sin\gamma_1. \quad \text{(A1)}$$

Conservation of area of the faulted and folded layer of the fault-propagation fold is derived by equating the area of three triangles (Fig. A1):

$$\Delta PQR = \Delta PQS + \Delta PST. \quad \text{(A2)}$$

The area of each triangle is given by

$$\Delta PQR = t^2(\cot\alpha + \tan\theta)/2 \quad \text{(A3)}$$

$$\Delta PQS = \Delta PQ'S - \Delta PQ'Q = t^2(\cot\gamma_1 - \tan\theta)/2 \quad \text{(A4)}$$

and

$$\Delta PST = \Delta PT'S - \Delta PT'T = tf^2(\cot\gamma_2 - \cot(180 - \alpha - \phi))/2, \quad \text{(A5)}$$

where the dip of the forelimb (ϕ) is related to the interlimb angle and the dip of the back limb according to

$$\phi = (180 - 2\theta - \gamma). \quad \text{(A6)}$$

Substituting equations (A3)–(A6) into (A2) and rearranging gives equation (3).

The equations defining the geometric relations for the fault-propagation fold are derived by combining equations (1) and (2) and expanding the terms $\sin(\gamma - \gamma_1)$ and $\sin(\gamma - \gamma_2)$ with the identity

$$\sin(X - Y) = \sin X\cos Y - \cos X\sin Y, \quad \text{(A7)}$$

to yield

$$\cot\gamma_1 = (tf/t + \cos\gamma)/\sin\gamma \quad \text{(A8)}$$

and

$$\cot\gamma_2 = (t/tf + \cos\gamma)/\sin\gamma. \quad \text{(A9)}$$

Equation (4) follows from substituting (A8) and (A9) into equation (3). For the simple-step fault propagation fold, the relation $2\theta = \alpha$ is substituted into equation (4) and combined with (A8) to yield

$$\cot\alpha + 2\tan(\alpha/2) - 2\cot\gamma_1 + \cot\gamma = 0. \quad \text{(A10)}$$

Equation (8) is derived from (A10) using the identities

$$\cos(\alpha/2) = (\sin\alpha)/2\sin(\alpha/2) \quad \text{(A11)}$$

and

$$\sin^2(\alpha/2) = (1 - \cos\alpha)/2. \quad \text{(A12)}$$

Equation (7) may be derived from equation (8) with the relation $\gamma = 2\gamma_1$, which describes the case of no thickening of the forelimb, and by substituting the identities

$$\cos(2\gamma_1) = 2\cos^2\gamma_1 - 1 \quad \text{(A13)}$$

and

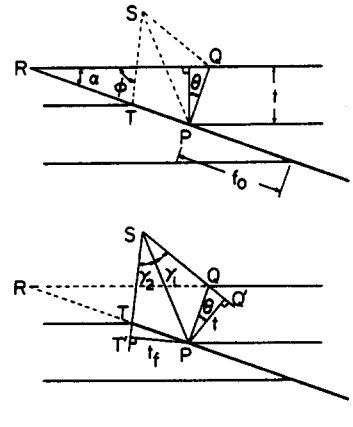

Fig. A1. Diagrams defining the areas of triangles and angles used to derive the geometric relations for the faulted and folded layers of the fault-propagation fold.

$$\sin \gamma_1 = (\sin 2\gamma_1)/2 \cos \gamma_1. \quad \text{(A14)}$$

Assuming that thickening in the forelimb is uniform, the dips of the axial surfaces A and A', as expressed in equation (5), are derived by rewriting equation (2) for the layers that are folded but not cut by the fault:

$$(tf/t) \sin \alpha^* = \sin (180 - \alpha^* - \phi) = \sin (2\theta + \gamma - \alpha^*). \quad \text{(A15)}$$

Equation (5) follows from equation (A15) by rearranging terms and expanding the term $\sin (2\theta + \gamma - \alpha^*)$ with the identity (A7).

The ratio of fault offset to thickness of the faulted layer (f_o/t) in equation (6) is derived by rearranging the terms in the following expression for the length of the fault segment TP (Fig. A1):

$$\text{TP} = t/\sin \alpha - f_o = tf/\sin (180 - \alpha - \phi). \quad \text{(A16)}$$